Carbon nanomaterials in biological systems

2007 J. Phys.: Condens. Matter 19 373101

(http://iopscience.iop.org/0953-8984/19/37/373101)

IOP PUBLISHING JOURNAL OF PHYSICS: CONDENSED MATTER

J. Phys.: Condens. Matter **19** (2007) 373101 (25pp) doi:10.1088/0953-8984/19/37/373101

TOPICAL REVIEW

Carbon nanomaterials in biological systems

Pu Chun Ke[1,3] **and Rui Qiao**[2]

[1] Laboratory of Single-Molecule Biophysics and Polymer Physics, Department of Physics and Astronomy, Clemson University, Clemson, SC 29634, USA
[2] Department of Mechanical Engineering, Clemson University, Clemson, SC 29634, USA

E-mail: pcke11@clemson.edu

Received 8 March 2007, in final form 9 March 2007
Published 27 July 2007
Online at stacks.iop.org/JPhysCM/19/373101

Abstract

This paper intends to reflect, from the biophysical viewpoint, our current understanding on interfacing nanomaterials, such as carbon nanotubes and fullerenes, with biological systems. Strategies for improving the solubility, and therefore, the bioavailability of nanomaterials in aqueous solutions are summarized. In particular, the underlining mechanisms of attaching biomacromolecules (DNA, RNA, proteins) and lysophospholipids onto carbon nanotubes and gallic acids onto fullerenes are analyzed. The diffusion and the cellular delivery of RNA-coated carbon nanotubes are characterized using fluorescence microscopy. The translocation of fullerenes across cell membranes is simulated using molecular dynamics to offer new insight into the complex issue of nanotoxicity. To assess the fate of nanomaterials in the environment, the biomodification of lipid-coated carbon nanotubes by the aquatic organism *Daphnia magna* is discussed. The aim of this paper is to illuminate the need for adopting multidisciplinary approaches in the field study of nanomaterials in biological systems and in the environment.

(Some figures in this article are in colour only in the electronic version)

Contents

[3] Author to whom any correspondence should be addressed.

1. Introduction

The past two decades have witnessed the rapid progress of nanotechnology, ranging from novel nanoelectronics to molecular assemblies, to nanocomposites, tissue engineering and biomedicine. Nanomaterials, because of their unique mechanical, thermal, and electronic properties, have reshaped many facets of modern science and engineering and are increasingly impacting our society, health care, and the environment. Within the realm of biotechnology, carbon nanotubes (CNTs), a major class of carbon-based tubular nanostructures, have been utilized as platforms for ultrasensitive recognition of antibodies [1], as nucleic acids sequencers [2], and as bioseperators, biocatalysts [3], and ion channel blockers [4] for facilitating biochemical reactions and biological processes. Towards nanomedicine, an emerging field of utilizing nanomaterials for novel and alternative diagnostics and therapeutics, CNTs have been utilized as scaffolds for neuronal and ligamentous tissue growth for regenerative interventions of the central nervous system and orthopaedic sites [5], substrates for detecting antibodies associated with human autoimmune diseases with high specificity [6], and carriers of contrast agent aquated Gd^{3+}-ion clusters for enhanced magnetic resonance imaging [7]. When coated with nucleic acids (DNA or RNA), vaccines, and proteins, CNTs have been shown as effective substrates for gene sequencing and as gene and drug delivery vectors to challenge conventional viral and particulate delivery systems [8–12].

Fullerenes, with C_{60} and C_{70} the most abundant, are spherically or elliptically shaped small carbon molecules whose graphitic backbones closely resemble those of CNTs. Fullerene research, most active during the 90s, is currently showing a reviving trend because of its relevance to the emerging fields of nanomedicine and nanotoxicity. Like CNTs, fullerenes also possess distinct structural, mechanical, optical, and quantum electronic properties which have applications in cell biology and drug therapy. Non-functionalized fullerenes, or bare 'buckyballs', can be widely distributed in all tissues, and can be retained in kidney, liver, bone, spleen, and excreted through urine and feces [13–15]. Due to their mutual *van der Waals* interaction, fullerenes readily accumulate, and their aggregates in cell membranes can facilitate electron transfer [16, 17], a phenomenon which may impact photosynthesis, metabolism, and drug delivery. To date, fullerenes have been employed as neuroprotective agents [18], HIV-1 protease inhibitors [19], antioxidants (one controversial topic regarding fullerenes) [20], x-ray contrast enhancers [21], and drug delivery transporters [22].

When incorporated into biological systems, the inert surface structures of carbon-based nanomaterials, CNTs and fullerenes in particular, may prevent their long-term bioavailability due to aggregation and settlement. Consequently, efforts to take advantage of the physical and chemical properties of CNTs and fullerenes in biological settings must first circumvent the hydrophobicity of these nanomaterials. Research over the past decade has shown that CNTs and fullerenes can be readily modified, either covalently or non-covalently, by incorporating chemical and biological functional groups for much enhanced solubility and

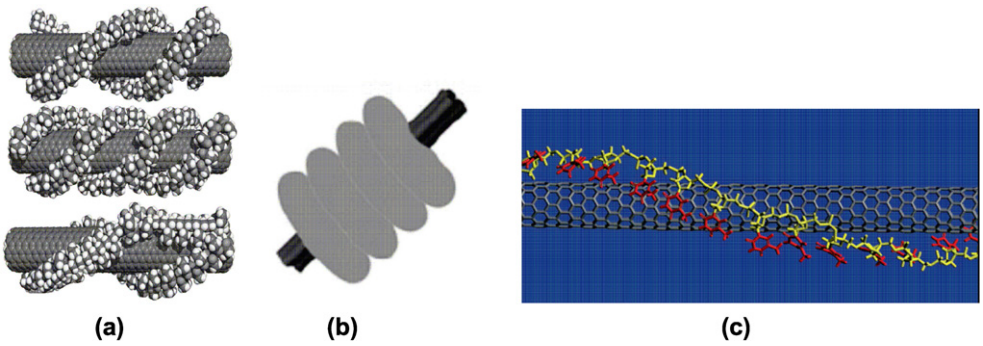

Figure 1. (a) Multiple helical wrappings of polymers on SWNTs [33] (© Elsevier); (b) continuous wrapping of polymer on an SWNT into 'stacks of pancakes' [40] (© American Chemical Society); and (c) ssDNA wrapping an SWNT with a chiral vector (10, 0) [37] (© Nature Publishing Group).

bioavailability. The covalent modification of single-walled carbon nanotubes (SWNTs), for example, normally involves esterification or amidation of acid-oxidized nanotubes and sidewall covalent attachment of functional groups [23–27]. However, these covalent schemes are often marred by undesirable modifications to the physical and chemical properties of SWNTs [28]. Furthermore, such functionalized SWNTs often have dangling bonds at the defective sites and are prone to generating free radicals. In comparison, the non-covalent modifications of SWNTs employ adsorption of proteins, biopolymers and synthetic polymers (DNA, RNA, polyvinyl pyrrolidone, polystyrene sulfonate), and surfactants (sodium dodecyl sulfate or SDS, etc) to form supramolecular assemblies [1, 29–37]. For both covalent and non-covalent solubilization schemes, the introduction of surfactants, surface charges, organic solvents and residues may induce additional cytotoxicity. Developing well-characterized solubilization schemes is thus crucial for facilitating the full range biological and biomedicinal applications of nanomaterials and their derivatives.

In the following sections, we elaborate on the biophysical mechanisms underlining the current non-covalent solubilization schemes, with a specific examination of the binding of lysophospholipids to SWNTs, the method developed in our lab [38]. We review research efforts using SWNTs and fullerenes as transporters for gene and drug delivery and exemplify our diffusion study of RNA delivery by SWNTs. We demonstrate the use of molecular dynamics for deciphering the binding of SWNTs and lysophospholipids and for predicting the translocation and cytotoxicity of fullerenes and their derivatives. We show that fullerenes, when coated with gallic acid an antioxidant and anticancer agent, can be used as robust fluorescence probes for imaging cells, tissues, and living organisms. To assess the biological and environmental impacts of water-soluble nanomaterials we further discuss the biomodification of lipid-coated SWNTs by aquatic organism *Daphnia magna* [39].

2. Supramolecular assemblies in aqueous solutions

2.1. Binding of synthetic polymers to SWNTs

Polymer wrapping was first proposed by Smalley *et al* as a non-covalent scheme for solubilizing tubular carbon nanostructures [33]. In this scheme, polyvinyl pyrrolidone (PVP), polystyrene sulfonate (PSS), or SDS bind to SWNT surfaces in a double helix, triple helix, multiple parallel wrapping, or 'stacks of pancakes' (figure 1) [40]. The wrapping of SWNTs by polymers was believed to be a general phenomenon, driven largely by thermodynamics to eliminate the

hydrophobic interface between the tubes and the aqueous medium. The entropic cost of turning a linear polymer into a coiled conformation was estimated as being, at most, that of restricting each polymer backbone bond to one of its three rotational minima, as [33]

$$\Delta S = -k \times \ln(W) = -k \times \ln(3^{n-2}),$$

where n is the number of backbone carbon atoms. To evaluate the thermodynamic driving force, the isoenergetic case was considered for polymers with favorable enthalpic interactions which resulted in a maximum free energy penalty for polymer conformational restriction at 25°C of 17 kJ mol^{-1} for per nm of wrapped SWNT. This penalty was offset by the loss of hydrophobic surface due to the shielding of the SWNT from water, estimated to be 136 kJ mol^{-1} for each nm of SWNT length at room temperature, calculated from the surface tension of the corresponding hydrophobic cavity. The free energy cost of forcing the polymeric wrapping into a regular wrapping arrangement is thus significantly smaller than the gain achieved by overcoming the hydrophobic penalty between the SWNTs and their surrounding water. It is proposed in this model that multiple wrapping is preferable to single continuous wrapping due to the lower cost of bending energy [33].

2.2. Binding of nucleic acids to SWNTs

Zheng *et al* described the binding of single-stranded DNA (ssDNA), specifically poly(T), to an SWNT as helical wrapping [37]. In this model ssDNA was treated as a flexible molecule with bond torsions within the sugar–phosphate backbone. This treatment is consistent with the wormlike-chain model that predicts the persistence length of ssDNA to be ∼1 nm at the physiological salt strength. Through simulations, Zheng *et al* determined that the flexibility of ssDNA allowed the molecule to seek low-energy conformations that maximized base–nanotube stacking while exposing the sugar–phosphate groups to water. The simulations also permitted the discovery of many possible binding modes, in which short ssDNA strands either bound to the SWNT surface in helical wrapping with both right- and left-handed turns, or simply adsorbed to the SWNT surface with a linearly extended structure. Figure 1(c) shows an overall right-handed helical wrapping of an ssDNA chain around an SWNT. Note that the bases are extended from the backbone and are pi-stacked onto the nanotube. In this configuration the sugar–phosphate backbone of the ssDNA is exposed to water and is easily solvated. For an ssDNA molecule to encase the nanotube and provide the hydrophilic sugar phosphate backbone on the exterior, a binding enthalpy of approximately −1.17 eV nm^{-1} is required. The entropic penalty can be estimated by treating each backbone torsion to be equivalent in solution, and by comparing the allowed conformations with the restrictions set on the nanotube surface, resulting in approximately 0.15 eV nm^{-1} at 300 K. This confirms that the enthalpy of binding is the dominant term in the binding free energy between ssDNA and an SWNT [37].

Our group was the first to investigate the non-specific binding of RNA polymers poly(rU) to SWNTs [34]. The major purposes of this study were to solubilize SWNTs for biocompatibility and use SWNTs for RNA delivery. Our non-specific binding mechanism for SWNTs and poly(rU), as opposed to the covalent binding schemes, offers more flexibility for releasing the load carried by SWNTs upon delivery. The structure of RNA, like that of DNA, comprises a negatively charged phosphate backbone and hydrophobic nitrogenous bases. The biological importance of RNA cannot be understated. For example: (1) messenger RNA (mRNA) are the transcripts of physical genes translated to functional proteins at the ribosomal level; (2) some RNA act as enzymes to catalyze a variety of cellular biochemical pathways, and serve as mediators for a variety of organic reactions, and as templates for the growth of inorganic particles; and (3) small interfering RNA (siRNAs), which disrupt mRNA

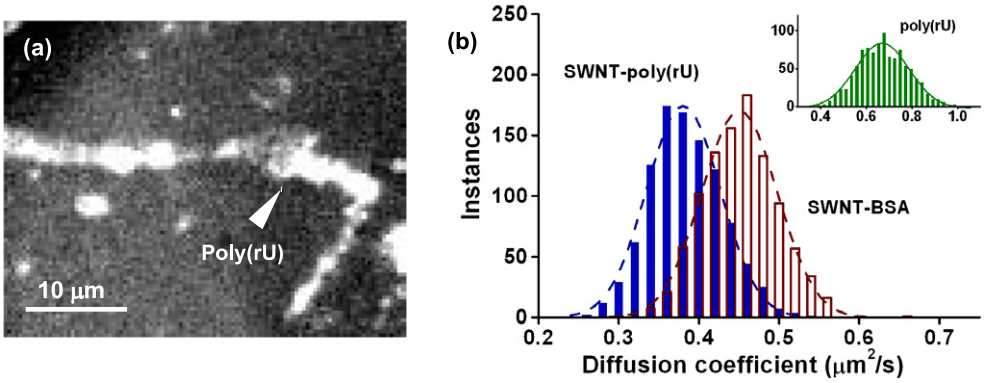

Figure 2. (a) Fluorescence image of SWNT–poly(rU) hybrids [34]. (b) Histograms of the diffusion coefficients of SWNT–poly(rU) (solid bar) and SWNT–BSA (empty bar) in TE buffer. BSA: protein bovine serum albumin. Inset: diffusion coefficient of poly(rU) in TE buffer [41] (© American Institute of Physics).

prior to translation, silence specific post-transcriptional gene expression for disease control and prevention [34].

Although our binding study was conducted in liquid, no helical wrapping was feasible as the CVD-produced SWNTs were pre-immobilized on a silicon substrate. The primary binding mechanisms in this study were the π-stacking between the bases of the poly(rU) and the π-electrons of the carbon atoms, and the hydrophobic interactions between the bases of the poly(rU) and graphitic surfaces of the SWNTs. Since poly(rU) was observed to be distributed along the contour of an SWNT (figure 2(a)), our results suggest that the π-stacking between the poly(rU) and the SWNT may dominate the hydrophobic and *van der Waals* interactions between both the poly(rU) bases and the silicon substrate [34].

With SWNTs solubilized by RNA polymer, we then characterized the diffusion of SWNT–poly(rU) in the aqueous solutions [41], which elicited information on the stability as well as the diffusion of the of SWNT–poly(rU) in liquid. For single-particle tracking, the trajectories of a fluorescent molecule can be followed at nanometer resolution based on Gaussian intensity profiling. The mean square displacement (MSD) of the center of mass (COM) of the molecule can be calculated as $\mathrm{MSD}(\Delta t) = \langle (x_{i+n} - x_i)^2 + (y_{i+n} - y_i)^2 \rangle$, where x_i and y_i are the coordinates of the COM of the molecule in frame i, and n denotes the frame number with a time interval Δt. The diffusion coefficient D of a molecule in two dimensions can be calculated as $D = \mathrm{MSD}/4\Delta t$ [41].

The diffusion coefficient for a small particle can be derived from Einstein's relation $D = k_\mathrm{B}T/k_\mathrm{drag}$, where k_B is the Boltzmann constant, T is the temperature, and k_drag is the drag coefficient of the solution. For an elongated particle, $k_\mathrm{drag} \propto \eta d$, where η is the viscosity of the solution, and d is the longest dimension of the particle (the average length of the SWNTs was 400 nm in our experiment). The stability/resolution of the imaging system, i.e., an EPI fluorescence microscope, was calibrated to be 5×10^{-5} $\mu\mathrm{m}^2$ s^{-1} with 2 μm fluorescent beads immobilized on a glass slide. As shown in figure 2, the diffusion coefficients of the SWNT–poly(rU) and the SWNT–BSA hybrids were measured to be 0.374 and 0.442 $\mu\mathrm{m}^2$ s^{-1}, respectively. These diffusion coefficients suggest that it would take approximately 1–2 min for a SWNT hybrid to diffuse across a cell of 10 μm in diameter, consistent with the known diffusion coefficients of DNA and proteins found in the cell's cytoplasm. By comparison, the diffusion coefficient of the poly(rU) alone (inset of figure 2) was found to be 0.661 $\mu\mathrm{m}^2$ s^{-1}, almost

twice as that for the SWNT–poly(rU) hybrids, possibly due to their different conformations. SWNT–poly(rU) hybrids exhibited a relatively smaller diffusion coefficient than SWNT–BSA because of the extrusion of poly(rU) from the SWNTs (the radius of gyration of BSA is ∼3 nm, two orders of magnitude smaller than that of poly(rU)) [41]. This experiment facilitated our translocation study of SWNT–poly(rU) across MCF7 cell membranes (section 3.1.2).

2.3. Binding of proteins to SWNTs

The interactions between a protein and a substrate (in both biological and non-biological terms) may involve forces that are electrostatic, hydrogen bonding, hydrophobic, or entropic in nature. These forces depend on the conformation of the protein, the surface charge of the substrate, and the pH, ionic strength, and temperature of the surrounding solution. Although there have been numerous studies done on protein adsorption, the interactions of nanomaterials with proteins, while still not well understood, have great relevance to the development of nanobiotechnology and nanomedicine.

The covalent binding of SWNTs with amino acids, the building blocks of proteins, was shown by Georgakilas *et al* [42]. The sidewalls of SWNTs or multiwalled carbon nanotubes (MWNTs) were functionalized with N-protected amino acids based on the 1,3-dipolar cycloaddition reaction. Huang *et al* attached protein BSA to SWNTs via diimide-activated amidation under ambient conditions [43]. In contrast, the non-specific binding or adsorption of proteins, while also solubilizing nanotubes, is generally less efficient than with nucleic acids. This is because the globular structure of a protein, as compared with the linear and flexible backbone of an ssDNA or a RNA molecule, hinders its seamless binding to a tubular SWNT and leaves large tube surface area exposed to water. Consistently, larger proteins such as fibrinogen (MW 340 kDa) show poorer binding to SWNTs than do smaller proteins such as streptavidin (MW 60 kDa) [29]. In the literature, binding of proteins and SWNTs is mostly employed for biomolecular recognition and sensing rather than SWNT solubilization. However, regardless of the application the non-specific binding of proteins to SWNTs is worth examining as it readily occurs when SWNTs, functionalized or not, are present in biological settings.

The specific binding of an anti-fullerene IgG monoclonal antibody to an SWNT was demonstrated by Erlanger *et al* based on an ELISA essay and atomic force microscopy (figure 3(a)) [44]. Another approach was demonstrated by Dai's group, in which the pyrene moiety of 1-pyrenebutanoic acid succinimidyl ester was pi-stacked with SWNT and the surface-immobilized esters were subsequently reacted with several proteins rich in surface amines [45]. Regarding the selective binding of protein such as streptavidin, Dai's group showed that surfactant Triton-X405 used as a wetting layer was pi-stacked with SWNTs. This pi-stacking enhanced the non-covalent adsorption of the amine-terminated poly(ethylene glycol) (PEG) polymer, resulting in a covalent binding of the amine-reactive biotin reagent to the PEG (figure 3(b)). The co-adsorption of Triton and PEG on SWNTs was found to be highly effective in preventing the adsorption of streptavidin on the nanotubes [29].

2.4. Binding of surfactants to SWNTs

Due to the large curvature and small diameter (0.8–2 nm) of an SWNT, amphiphiles such as SDS, Triton X-100, Pluronic F108, and phospholipids are often more advantageous than macromolecules such as linear polymers, proteins, and nucleic acids in rendering SWNTs water soluble. The use of SDS, a negatively charged surfactant, introduced by Smalley *et al*, has found many applications in the photoluminescence of SWNTs and in the optical detection of SWNT translocation (figure 4) [32, 46].

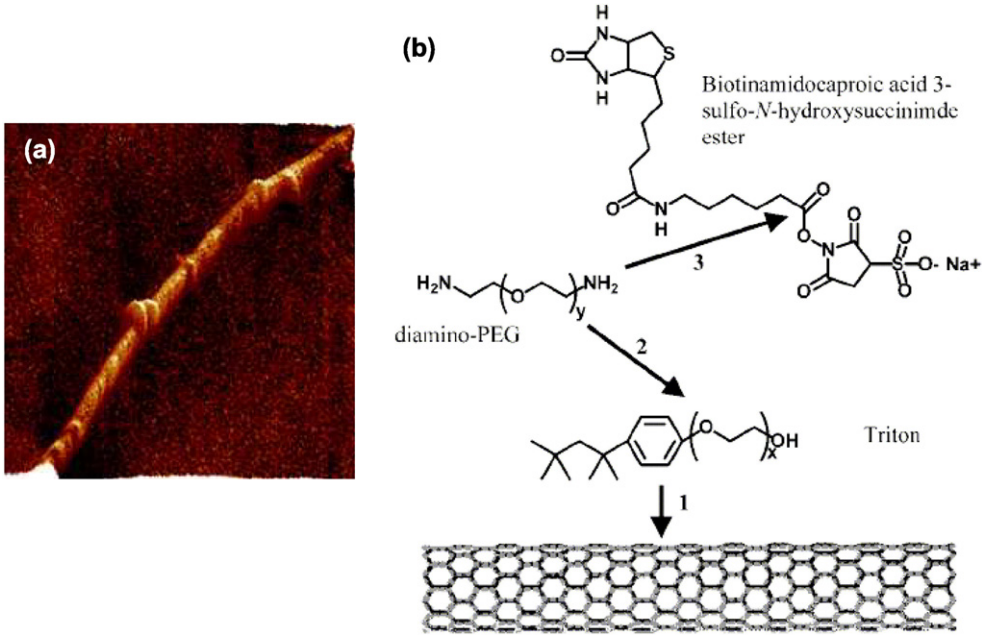

Figure 3. (a) Atomic force microscopy image of an SWNT with fullerene-specific antibody [44]. (b) Triton-X 405 adsorbed on an SWNT followed by amine-terminated PEG covalently linked to biotin [29] (© American Chemical Society).

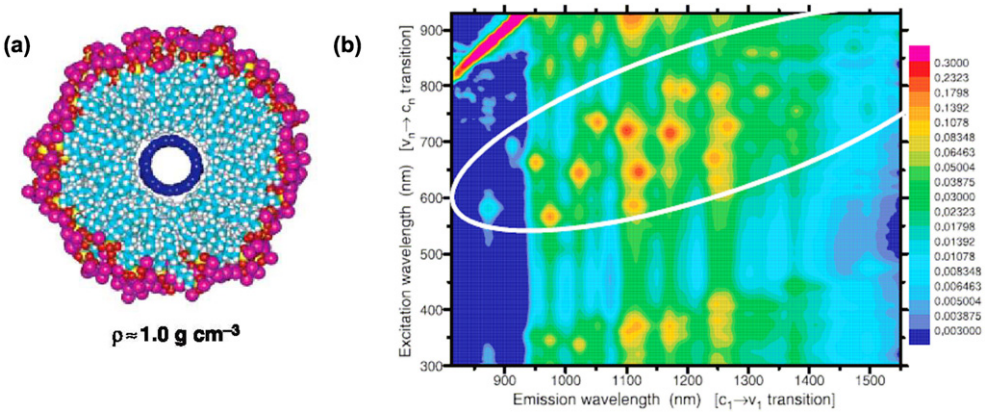

Figure 4. (a) Cross-sectional model of an individual SWNT in a cylindrical SDS micelle. The approximate density of the SWNT–SDS is 1.0 g cm^{-3} [32]. (b) Contour plot of fluorescence intensity versus excitation and emission wavelengths for a sample of SWNTs suspended in SDS and deuterium oxide [46] (© American Association for the Advancement of Science).

We have recently demonstrated the use of zwitterionic lysophosphotidylcholine (LPC) for solubilizing SWNTs in aqueous solutions [38]. We have noticed this method is more effective than with nucleic acids, and far more effective than with proteins and SDS. The remarkable solubility of SWNTs, coupled with the biocompatibility of lysophospholipids (signaling molecules in cell membranes), may facilitate research on biological responses to

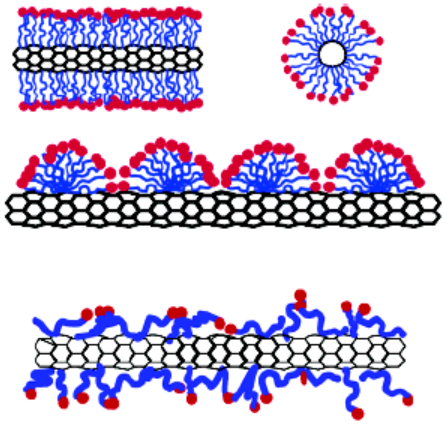

Figure 5. Schematic representations of the mechanisms by which surfactants help disperse SWNTs. (Top) SWNT encapsulated in a cylindrical surfactant micelle. (Middle) Hemimicellar adsorption of surfactants on an SWNT. (Bottom) Random adsorption of surfactants on an SWNT [31] (© American Chemical Society).

nanomaterials and on assessing the environmental impact of nanomaterials. Furthermore, the superior solubility afforded by LPC may benefit the development of single-nanoparticle chemical and biosensors and nanodevices. Obviously, understanding the workings of SWNT–amphiphile assembly is of great importance for these applications.

2.4.1. Three models. Natural and synthetic surfactants are amphiphiles in that they possess both hydrophobic and hydrophilic moieties. Under certain conditions, amphiphiles can self-assemble into functional structures such as liposomes, polypeptides, proteins, DNA, and RNA, and further compile into molecular machines and membranes via covalent and non-covalent forces. Understanding the interactions between amphiphiles and cylindrical nanostructures underlines both the solubilization of nanotubes and the design of novel nanostructures and molecular complexes. Three models, i.e., cylindrical micelle, hemimicelle, and random adsorption models (figure 5) have been documented in the literature. Each are supported by experimental studies using absorption spectroscopy, small-angle neutron scattering (SANS), fluorescence microscopy, transmission electron microscopy (TEM), and theoretical studies using molecular simulations [30, 31, 38, 47]. However, these studies are wholly incompatible and the 'true' binding mode of cylindrical nanostructures and amphiphiles is unclear.

2.4.1.1. Cylindrical micelle. The cylindrical micelle model was supported by experimental study on the dispersion of SWNTs in surfactant sodium dodecylbenzenesulfonate (NaDDBS) [30]. The electrical charge of SWNT surface varied with the pH of the surrounding media, while the Coulombic forces between the anionic NaDDBS and the SWNT were dominated by the hydrophobic interaction between the surfactant tail and the nanotube sidewall. This study found that NaDDBS encased nanotubes through a two-step adsorption process that eventually results in a surfactant monolayer. Although the final conformation of this monolayer is no different from inserting a nanotube into a surfactant micelle, the binding energy and the dynamics of these two processes fundamentally differ [30]. This model was supported by the molecular dynamics simulations by O'Connell *et al* [32] (figure 4(a)).

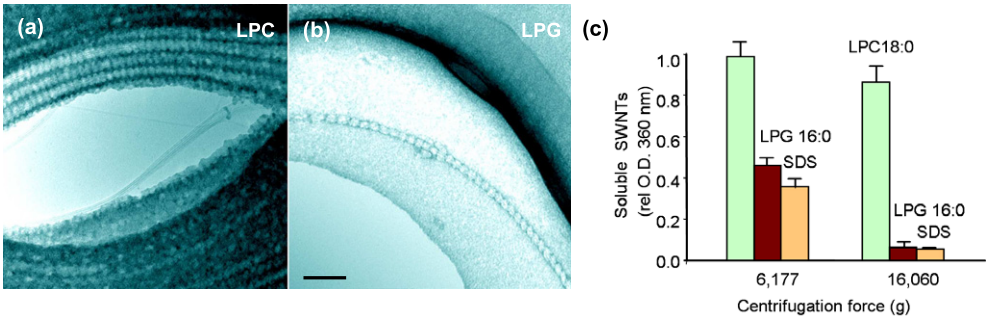

Figure 6. TEM images of (a) SWNT–LPC and (b) SWNT–LPG complexes. Note the SWNT–LPG striations are less organized and wider than SWNT–LPC. Scale bar: 20 nm. (c) SWNT solubility in LPC, LPG, and SDS solutions, respectively [38] (© American Chemical Society).

2.4.1.2. Hemimicelle. Richard *et al* provided strong experimental evidence that supports the hemimicellar binding model [47]. Based on their TEM and cryo-TEM studies of SDS and other synthetic lipids interacting with SWNTs and MWNTs, they determined that only SDS at above its CMC formed rolled-up half-cylinders on the nanotube surface. Depending on the symmetry and the diameter of the carbon nanotube, these studies also recorded rings, helices, and double helices. Similar self-assemblies on carbon nanotubes were recorded for both single-tailed and double-tailed synthetic lipids that were found to be contradictory to our experimental observations (section 2.4.2) [38]. Since cryo-TEM involves solvent sublimation, it remains uncertain as to what degree these ordered structures in the vacuum phase truly manifest their states in the liquid phase.

2.4.1.3. Random adsorption. Yurekli *et al* found no preferential arrangements for the head and tail of SDS in dispersing SWNTs [31]. Their SANS experiment showed no agreement with the cylindrical micelle model for SDS either below or above its critical micelle concentration (CMC). Based on these findings and their assumption that hemimicellar binding was 'sterically and energetically unfavourable', Yurekli *et al* proposed the random adsorption model—the arrangement of a structureless, adsorbed layer of surfactants on individual nanotubes.

2.4.2. SWNT–lysophospholipid assembly

2.4.2.1. TEM and spectrophotometry studies. We recently observed that single-tailed lipids, not double-tailed lipids, coated SWNTs as striations whose size and regularity were affected by the polarity of the lipids [38]. While we determined that the LPC striations along the tube(s) remained approximately the same size (figure 6(a)), the size and orientation of negatively charged lysophosphatidylglycerol (LPG) striations varied in size along the tube axis (figure 6(b)). This size variance was because the charge repulsion between the LPG head groups prevented compact packing on the SWNTs. In contrast, zwitterionic LPC carried a large dipole moment, which permitted a tight packing of tube surface and a better lipid–water interaction. At 16 060 g, LPC is at least one order of magnitude more effective than either SDS or LPG in dispersing SWNTs (figure 6(c)). This increase in effectiveness was because LPC had a bulkier head group for interfacing with water and a longer acyl chain for binding to SWNTs [38].

In figures 6(a) and (b), the organizations of LPC and LPG striations resemble those of SDS and synthetic lipids observed on carbon nanotubes by Richard *et al*. However

none of the double-tailed phospholipids we have tested, i.e., phosphotidylcholine PC 24:0 (zwitterionic), phosphatidylglycerol PG 36:2 (negatively charged), and phosphoethanolamine PE 32:0 (negatively charged), yielded a good SWNT solubility at physiological pH. From a geometrical standpoint, double-tailed phospholipids are more curvophobic; their structures can be approximated as cylinders and their packing assumes planar bilayers. Thus, wrapping around a cylindrical SWNT is not geometrically preferable for phospholipids [38].

2.4.2.2. Temperature dependence. We conducted temperature dependence measurements of an SWNT–LPC assembly in water. The temperature was increased from 7 to 95 °C with no noticeable absorbance change observed. This temperature dependence of SWNT–LPC assembly provided evidence that SWNTs and LPC bound tightly and acted as single entities as a whole, rather than dynamic equilibria of supramolecular associations in solution. This finding is important for the design and applications of SWNT–lipid assembly.

2.4.2.3. Stability and salt dependence. We examined the salt dependence of surfactant-coated SWNTs. LPC, SDS and DOPA (3,4-dihydroxy-L-phenylalanine) were respectively mixed at a weight ratio of 5:1 with SWNTs and dispersed in distilled water through probe sonication. The initial concentration of SWNT was 1 mg ml^{-1} for all three samples. After 30 min of sonication, the solutions were centrifuged at 7500 rpm for 3 min and the supernatants were collected for absorbance measurements. As shown in table 1(a), there was little settlement for SWNT–LPC after the centrifugation, while both SWNT–SDS and SWNT–DOPA underwent significant precipitation. The UV absorbance of the three SWNT solutions was read at 360 nm and normalized based on the absorbance of SWNT–LPC. The SWNT solutions were stored at room temperature and their absorbance measured on the first day, the fourth day, the fifth day, and the sixth day. SWNT–LPC showed the highest solubility on all four test days (table 1(a)).

NaCl and $CaCl_2$ of 20 mM were added to the three SWNT solutions. Approximately 20% decreases were determined for all three samples with the addition of NaCl. However, SWNTs started to precipitate markedly once calcium ions were added to either SWNT–SDS or SWNT–DOPA solution. Table 1(b) tabulates the UV absorbance taken one day after the salt additions. SWNT–LPC solution is shown as the most stable and the least sensitive to the change of ionic strength possibly due to the neutrality of the LPC molecules. In comparison, the binding of negatively charged SDS or DOPA onto SWNTs was much more prone to the presence of ions, possibly because the ions altered the equilibrium between SDS or DOPA micelle formation and the their packing on the SWNTs. In other words, since the surfactants were shielded by the ions, their mutual interactions and their binding to SWNTs could become energetically less favorable. We therefore conclude the SWNT solubility depends upon the polarity of surfactants and the ionic strength of the solution.

2.4.2.4. MD simulations on SWNT–lipid assembly. Although experimental characterization of the SWNT–lipids self-assembly can provide considerable insight into the mechanisms of SWNT solubilization, such characterization is limited by the imaging resolution. In particular, the exact binding mode of lipids on the SWNT cannot be established without ambiguity. In such cases, molecular dynamics (MD) simulations can be advantageous as it allows the SWNT–LPC self-assembly to be resolved with atomistic resolution. We performed MD simulations to elucidate the binding of LPC on an SWNT [48]. A single (18, 0) SWNT (diameter: 1.4 nm, length: 11.8 nm) was fixed at the center of the simulation box and 76 LPC molecules were distributed roughly uniformly within the box at the beginning of the simulation. As

Table 1. (a) Stability of SWNT–LPC, SWNT–SDS, and SWNT–DOPA over time. (b) Absorbance of SWNT–LPC, SWNT–SDS, and SWNT–DOPA in the presence of Na^{+} and Ca^{2+} ions.

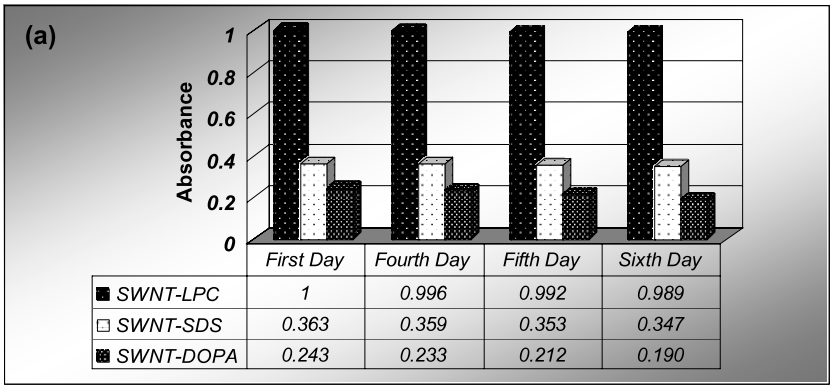

	First Day	Fourth Day	Fifth Day	Sixth Day
SWNT-LPC	1	0.996	0.992	0.989
SWNT-SDS	0.363	0.359	0.353	0.347
SWNT-DOPA	0.243	0.233	0.212	0.190

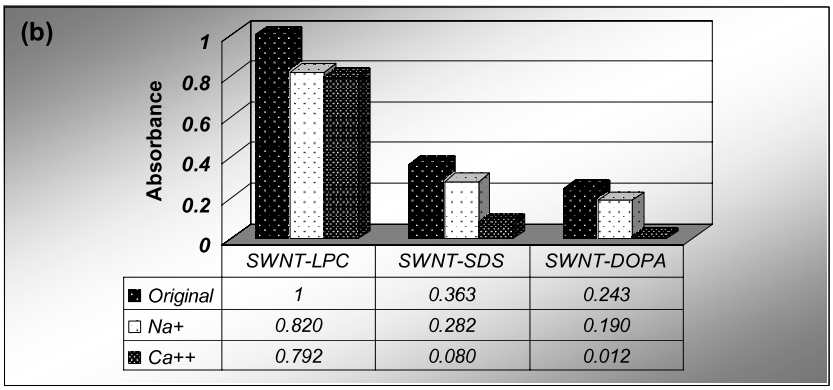

	SWNT-LPC	SWNT-SDS	SWNT-DOPA
Original	1	0.363	0.243
Na+	0.820	0.282	0.190
Ca++	0.792	0.080	0.012

hydrophobic interaction is the major driving force for the formation of SWNT–LPC self-assembly, water was modeled explicitly. The system consisted of a total of 45 013 atoms. The system was simulated in the NPT ensemble ($T = 300$ K, $P = 1$ bar) by using the Gromacs package [49] for 24 ns.

The simulation indicated that the lipids readily adsorbs onto the SWNT. While a large fraction of the lipids bind onto the SWNT in a one-by-one fashion, some first formed clusters in the bulk and adsorbed onto the SWNT collectively. Upon adsorption onto the SWNT, the cluster slowly underwent a series of conformation change. Figure 7(a) shows a side view of the simulation system at $t = 24$ ns, with large fractions of the lipids organized into 'half-cylinders' that wrapped the SWNT spirally. The periodicity of the wrapping along the tube axis is ∼4.5 nm, in good agreement with our TEM study of SWNT–LPC self-assembly (figure 7(c)). Although the conformation of the LPC adsorbed on the SWNT bears some similarity to the hemi-micelles binding proposed in [50], there are fundamental differences. Specifically, instead of stemming out of a central core like surfactants in a micelle, the 'crests' in figure 7(a) actually consist of several lipid layers (see figure 7(b)) shifted along the tube axis and packed in parallel and anti-parallel directions. The lipid tails are shielded by their head groups at the outer rims of the 'crests', resulting in good SWNT solubility. A further analysis of the alignment of LPC molecules indicate that the LPC molecules are predominantly aligned along the SWNT axis,

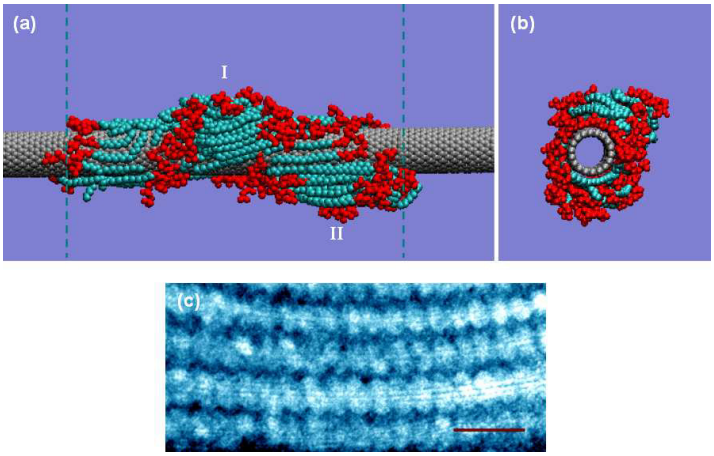

Figure 7. Self-assembly of LPC and an SWNT. (a) Frontal view of the simulation system configuration at $t = 24$ ns. The lipid bump I is formed from the gradual adsorption of lipids from the bulk while the lipid bump II is formed from the adsorption of a lipid cluster from the bulk. The lipid head groups and the tails are illustrated in red/dark beads and cyan/light chains and the SWNT is in gray/cylinder, respectively. The dashed lines in (a) denote the periodic boundary of the simulation box (∼12 nm). (b) Side view of the SWNT–LPC simulation system (water not shown). Image rendered by using VMD. (c) TEM image of SWNT–LPC assemblies display a striation periodicity of ∼4.5 nm. Scale bar: 15 nm [48] (© American Chemical Society).

in contrast to that depicted by the 'cylindrical surfactant encapsulation' [33] or the 'random adsorption' [31] models.

The key factors leading to the binding pattern shown in figure 7(a) are the hydrophobic nature of SWNT and the large curvature of the SWNT. Specifically, in the beginning of the binding process when the lipid coverage of the SWNT surface was low, lipids were readily adsorbed on the SWNT surface. The lipids tend to align with the tube axis as wrapping SWNT with a very small radius is energetically costly. Such an alignment also maximizes the contact between lipids and the hydrophobic SWNT surface. The cylindrical encapsulation model and the random adsorption model cannot explain the striations observed in the TEM experiments. The hemi-micellar model requires lipid micelles to break from the middle and then to assemble in tandem on an SWNT. In comparison, our illustrated mechanism agrees with the TEM experiments [1, 2] and is sterically and energetically favorable for the self-assembly of amphiphiles and cylindrical nanostructures.

While the above MD simulation provides new insights into the self-assembly of amphiphiles and SWNT, a significant amount of work remain to be done. For example, detailed characterization of the binding affinity of LPC on SWNT will help to understand elucidate the stability of the self-assembly. Moreover, studies of the binding of charged amphiphiles onto SWNT under various ionic concentrations may explain the different stability of lipid amphiphile–SWNT self-assembly, as shown in table 1. The fundamental understanding of lipid amphiphile–SWNT self-assembly derived from such studies will help to improve the biocompatibility of nanomaterial and to facilitate the design of new nanostructures and molecular complexes for supramolecular chemistry.

2.5. Binding of gallic acids to fullerene C_{70}

Because of their inert surface structures, fullerenes are only weakly soluble in water. We have devised a solubilization scheme by coating C_{70} with phenol gallic acid $C_7H_6O_5$ (structure see

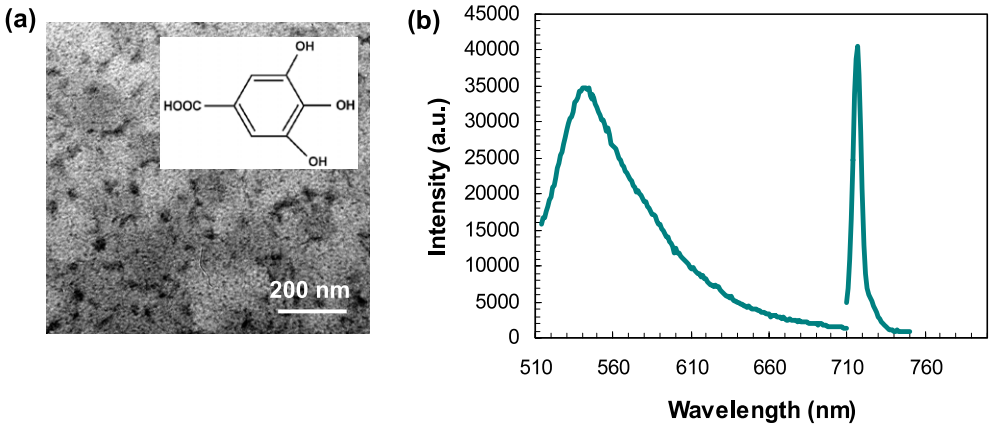

Figure 8. (a) TEM image of C_{70}–gallic acid complexes. (b) Fluorescence of C_{70}–gallic acid at ∼540 nm and 719 nm excited with 488 and 690 nm, respectively. The concentration of C_{70} is 1 mg ml^{-1} and the weight ratio of C_{70}–gallic acid is 1:20.

figure 8(a) inset). The UV absorbance of C_{70}–gallic acid was measured at 384 nm where a saturation concentration was found at ∼1 mg ml^{-1}. We postulated that C_{70}–gallic acid complexes were assembled via pi-stacking and their solubility afforded by the polarity of the gallic acid. The solubility of C_{70}–gallic acid could also be elicited by gallic acid which caged C_{70} via hydrogen bonds, much like water molecules caging fullerenes [51]. We removed free gallic acid and larger C_{70} or C_{70}–gallic acid aggregates through consecutive filtrations and found the sizes of the resulting C_{70}–gallic acid were mostly within 10–20 nm. Additional NMR studies showed no spectral signatures for C_{70}–gallic acid due to the non-covalent nature of the binding and the randomness of the complex size due to *van der Waals* interaction. The solution of C_{70}–gallic acid displayed a light green color and was stable for weeks at room temperature.

Both C_{60} and C_{70} absorb strongly in the ultraviolet region, though C_{70} has a higher absorption than C_{60} in the visible regions, possibly due to its elongated form and reduced symmetry [52, 53]. C_{60} and C_{70} are known to be soluble in organic solvents such as toluene or benzene which can be photoexcited to induce weak fluorescence from visible to near infrared [52–56]. Concomitantly we have recorded the fluorescence of C_{70}–gallic acid in water which exhibited two distinct peaks at ∼540 and 719 nm, and attributed the former to well solubilized C_{70}–gallic acid and the latter to large C_{70} aggregates (figure 8(b)). Using this approach we also solubilized C_{60}. However, the fluorescence of C_{60}–gallic acid was noticeably weaker, broader, and less distinctive than their C_{70} counterpart, possibly because the fluorescence emission of C_{60} extends further into the near infrared region. Such water-soluble fullerenes are biocompatible due to the antioxidation and anticancer properties of the gallic acid [57, 58]. The solubility elicited by gallic acid may facilitates future studies of fullerene uptake and toxicity.

3. Bioapplications of solubilized nanomaterials

3.1. Gene and drug delivery

One of the greatest challenges for gene delivery is the physicochemical properties of DNA such as its negative charge and hydrodynamic volume. As a result DNA cannot be taken up

by cell membranes without the aid of transporters or 'vectors'. Current solutions include viral and non-viral transfection vectors such as cationic lipids [59], polyethylenimine (PEI), and other cationic polymers [60, 61]. The viral transfection vectors are the most effective due to their natural ability to invade cells. However, they often provoke immune responses from cells which prevent long-term gene delivery. Non-viral vectors may avoid immune responses but are often hindered by low uptake and gene expression efficiencies [62].

As none of these current vectors are ideal, alternatives must be developed. SWNTs are one such alternative. They are promising candidates in that they have large surface areas, high stability and flexibility, and can be covalently or non-covalently functionalized for improved biocompatibility and bioavailability. Recently, Pantarotto *et al* determined that fluorescently labeled SWNTs covalently bound with bioactive peptides could penetrate through cellular and nuclear membranes [8]. Kam *et al* reported the uptake of SWNT–streptavidin conjugates within promyelocytic leukemia and T cells [10]. The mechanisms proposed for SWNT cellular uptake include phagocytosis, endocytosis, insertion, and passive diffusion.

3.1.1. DNA delivery. The Pantarotto study [9] showed that both SWNTs and MWNTs were covalently modified by pyrrolidine rings, each bearing a free amino-terminal oligoethylene glycol moiety attached to the nitrogen atom. The presence of these functional groups led to a much increased solubility of the CNTs in aqueous solution. Plasma DNA, encoded with marker gene (β-galactosidase; β-gal), was attached to positively charged ammonium functionalized CNTs via electrostatic interaction. Nuclear localization and translocation of CNTs through plasma cell membranes were observed with TEM. The mechanism hereby was thought to be the binding of the cationic functional groups on the CNTs to the cell membranes, which could be facilitated by spontaneous insertion of the CNTs across the cell membranes. Subsequent translocation and diffusion of the functionalized CNTs within the intra-cellular space could occur following these nonendocytotic processes. The rate of gene transfection was found to be dependent on the charge ratio of the ammonium groups on the SWNT surface to the phosphate groups of the DNA backbone. Gene expression efficiencies of 5–10 times higher than those without the presence of SWNTs were obtained. Gene expression also increased with incubation time of up to 3 h and decreased thereafter. No significant cytotoxicity was reported [9].

3.1.2. RNA delivery. We were the first to demonstrate the translocation of the RNA polymer by SWNT transporters [12]. Using the sectioning property of confocal fluorescence microscopy, we located fluorescently labelled SWNT–poly(rU) hybrids on cell membranes, either within the cytoplasm or in the nuclei of MCF7 breast cancer cells. We also performed radioisotope labelling, cell enumeration, and MTS assay, which measures cellular metabolic activity through absorption. These studies provided information on the direct cellular uptake and the cytotoxicity of SWNTs. Figure 9 shows the sectioning images of MCF7 cells incubated with SWNT–poly(rU) for 3 h. In (a), the fluorescent poly(rU) molecules were spotted on the cell membrane and in the cytoplasm. In (b), the fluorescent spot was co-localized with the nucleus, which supports the possibility that the SWNT–poly(rU) hybrid could have penetrated through the nuclear membrane. The observed fluorescence in figure 9 could also be from propidium iodide (PI)-labelled poly(rU) released from SWNTs due to dissociation kinetics of the hybrids. It should be pointed out that from the energetic viewpoint, the fluorescence in the nucleus is unlikely to be from either free PI or PI dissociated from poly(rU), which is then re-intercalated with the host DNA or RNA. The strong fluorescence in figure 9(b) fades gradually in the other cross sections (data not shown), further indicating that the SWNT–poly(rU) hybrid was localized within the cell [12].

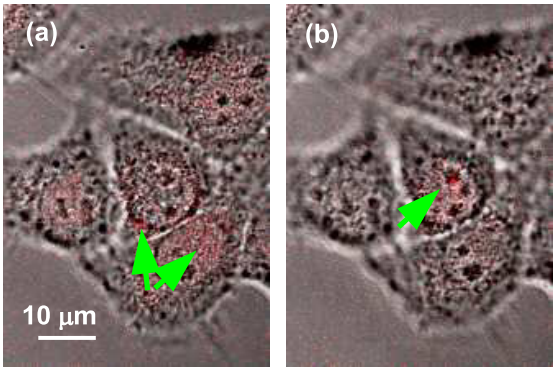

Figure 9. Confocal fluorescence images of MCF7 cells incubated with 0.05 ml ml^{-1} of PI-labelled SWNT–poly(rU) for 3 h. The arrows point to large fluorescent SWNT–poly(rU) hybrids (a) on cell membrane and in cytoplasm and (b) in cell nucleus [12].

We postulated that the uptake of the SWNT–poly(rU) was due to the amphipathic properties of both the cellular membranes and the SWNT–poly(rU) hybrids. The passive diffusion of membrane phospholipids and the hybrids, as well as the telophase of cell mitosis could also encase SWNTs. Both our cell growth and MTS studies showed no cytotoxicity in either MCF7 breast cancer cells or d2C keratinocytes for SWNT of concentrations up to 1 mg ml^{-1} [12].

In one of the most exciting developments thus far, Dai's group reported gene silencing with SWNT delivery [63]. The delivered siRNA was capable of silencing the gene encoding lamin A/C protein. Phospholipids (PL) were adsorbed onto SWNTs and the head groups of the PL were covalently linked to single-chained poly(ethylene glycol) (PEG) with terminal amine or maleimide groups (PL–PEG–NH_2 or PL–PEG–maleimide). The PL–PEG bound to SWNTs via *van der Waals* and hydrophobic interactions between the fatty alkyl chains of the PL and the sidewalls of the SWNTs. Although double-chained PL molecules alone did not solubilize SWNTs, the presence of the PEG greatly increased the hydrophilic moiety of the PL–PEG–SWNT complexes, rendering SWNTs water soluble. In the silencing assay, PL–PEI functionalized SWNTs transported siRNA into HeLa cells, and the disulfide bonds linking the siRNA and the phospholipid–PEI were cleaved off by the enzymes in acidic lysosomes. The translocation of SWNT complexes across cell membranes was hypothesized to result from endocytosis and no adverse effect on cell viability or proliferation was found in the presence of SWNTs. The silencing potency using siRNA, a twofold increase as compared with commercial lipofectamine delivery, was attributed to the high surface area and high intracellular transporting ability of SWNTs, as well as the high degree of endosome/lysosome escape after the cleavage of the disulfide bond [63].

3.1.3. Protein delivery. Kam *et al* explored protein delivery with SWNTs [64]. The streptavidin (SA), protein A (SpA), BSA, and cytochrome *c* (cyt*c*) proteins were fluorescently labeled and bound to the sidewalls of SWNTs via adsorption. The translocation of these proteins in mammalian cell lines, including HeLa, NIH-3T3 fibroblast, HL60, and Jurkats cells, were observed with confocal fluorescence microscopy. Lowering temperature to 4 °C yielded little uptake, indicating that endocytosis was responsible for the uptake of nanomaterials at room temperature [64].

Cellular uptake of large proteins (MW $>$ 80 kDa) was poor, while the intra-cellular transport of proteins by SWNTs appeared to be general for small- and medium-sized proteins.

SWNT–protein conjugates, once internalized within the cells, were co-localized with the red endocytosis endosome marker FM 4-64; suggesting the confinement of the conjugates in endosomal lipid vesicles. NIH-3T3 cells are known to undergo cyt*c*-induced apoptosis which can be analyzed using FITC-labelled Annexin V, an efficient marker for early stage apoptosis. Indeed, significantly higher percentages of apoptosed cells were observed for NIH-3T3 cells incubated with cyt*c*-SWNT conjugates than with cyt*c* alone [64].

To investigate the effect of endosomal release on the efficiency of apoptosis induction by cyt*c*, cells were incubated with cyt*c*-SWNT in the presence and absence of chloroquine, a membrane-permeable base that can localize inside endosomes and cause increases in pH. Higher degrees of apoptosis were observed for cells treated with cyt*c*-SWNT in the presence of chloroquine. This higher degree of apoptosis is due to the more efficient endosomal releasing of proteins, suggesting that the cyto*c* transported by SWNTs remained biologically active for apoptosis induction. However, it is unclear if the functionality of cyto*c* was retained after detached from the SWNTs, or if it remained active even when proteins were still attached to the SWNTs [64].

3.2. Sensing and imaging

SWNTs show distinct photophysical properties, such as fluorescence, which are only available at the single-particle level [32, 46]. These properties may be used for sensing DNA polymorphism, imaging nanoparticle translocation, or for developing new cancer therapeutics. Kam *et al* demonstrated a scheme for the selective destruction of cancer cells [65]. In this scheme, SWNTs were conjugated with various phospholipids (PL), a polyethylene glycol (PEG) moiety, and a terminal folic acid (FA) group that provided specificity for folic acid-starved HeLa cells. SWNTs conjugated with the folate moiety were internalized by the cells and were consequently irradiated with a near infrared laser to induce the first and second van Hove optical transitions of the isolated tubes [46]. The optical stimulations of SWNTs, transferred to molecular vibration energies and heat within minutes, eventually destroyed folate-starved cancer cells. Healthy cells without folate deprivation showed little SWNTs translocation and remained viable due to the biocompatibility of the near infrared wavelength.

Heller *et al* observed a red shift of the SWNT band-gap fluorescence when an encapsulating 30-nucleotide oligomer was exposed to counter-ions that screened the charged DNA backbone [66]. The transition was thermodynamically identical for DNA on and off the nanotube, except that the propagation length of the former was shorter by five-sixths. Based on the fluorescence profiles of SWNTs Heller *et al* characterized the B to Z conformational transition of DNA on the nanotubes in the presence of divalent chloride counter-ions. This remarkable transducing capacity of SWNTs, can in principle, be used for ion detection in media already possessing a strong ionic background [66].

We have recently devised a scheme to detect lipid delivery based on the physical mechanism of fluorescence resonance energy transfer, or FRET, in which a laser excited rhodamine–lysophosphoethanolamine (Rd–LPE) molecule donates its absorbed energy to an acceptor, an SWNT [67]. The absorption spectrum of isolated SWNTs overlapping with the emission spectrum of rhodamine makes this possible (refer to figure 4(b), excitation at 585 nm induces a fluorescence emission of isolated SWNTs at 985 nm). Furthermore, Rd–LPE can readily solubilize SWNTs because of its polar moment and conical shape. In our experiments, we observed that the fluorescence of Rd–LPE was quenched when it was mixed with SWNTs caused by FRET. Conversely, the fluorescence of Rd–LPE was recovered when the lipids were stripped off SWNT by washing with coloform. This ‘optical switch’ enabled our monitoring of SWNT–lipid delivery and their binding and dissociation in cells.

We imaged the translocation of Rd–LPE–SWNT complexes across MCF7 breast cancer cells. The cells were largely fluorescent after 3 h of incubation, suggesting a high uptake rate of the complexes and the separation between SWNTs and Rd–LPE after their translocation. This scheme, which denotes the ready release of drug loads off their SWNT transporters, may be useful for developing new delivery schemes using SWNTs. In additional experiments, we further observed that the fluorescence of Rd–LPE was non-uniformly distributed inside cells and primarily outside cell nuclei. This observation, combined with the principle of FRET, suggests that SWNTs were stored in certain cell compartments after their translocation [67].

4. Biological responses to carbon nanomaterials

Mitigating cytotoxicity, which is an integral part of the biological responses to nanomaterials, is a continuous concern in the development of new nanotechnologies. Fundamental studies in this area are critical to gaining a thorough understanding of the biological and environmental effects of nanomaterials and are becoming increasingly important due to the growing presence of nanomaterials. Shvedova *et al* determined that transition metal catalysts such as iron and nickel at SWNT concentrations of 0.06 mg ml^{-1} and higher were toxic to human epidermal keratinocytes [68]. Inhaling SWNTs have been found to cause the growth of granulomas in the lungs of rats, which had a total absence of such pulmonary biomarkers as inflammation, cell proliferation, and cytotoxicity [69, 70]. Colvin's group revealed that C_{60} was more toxic to human skin cells than $C_{60}(OH)_{24}$, and fullerenes with higher degrees of surface modifications became less toxic due to their inability to generate oxygen radicals [71]. This study was supported by our recent simulations on the translocation of fullerenes and their derivatives across a lipid bilayer [72]. Pantarotto *et al* found that 90% of fibroblasts remained alive when incubated with SWNTs of 5 μM [8]. Kam *et al* reported that promyelocytic leukemia cells were viable when the SWNT concentrations were below 1.25 μM [10]. Colvin *et al* reported that the toxicity of SWNTs to human dermal fibroblasts decreased as the functionalization of the tubes was increased [73]. We observed no significant difference in cell growth for MCF7 or d2C cells over a 3 day period with and without SWNTs of up to 1 mg ml^{-1} [12]. Manna *et al* reported increased oxidative stress and inhibition of cell proliferation in response to treatment of human keratinocytes with SWNTs [74]. They suggested that SWNTs activated Nuclear Factor-kappa B (NF-κB), a known transcription factor, in a dose-dependent manner in keratinocytes. Furthermore, Manna *et al* suggested that the activation of NF-κB was due to the activation of stress-related kinases by SWNTs in keratinocytes. Singh *et al* studied the tissue biodistribution and blood clearance rates of intravenously administered SWNTs which were covalently functionalized with chelating molecule diethylentriaminepentaacetic (DTPA) and radiotracer indium (^{111}Ln) [75]. They determined that none of the reticuloendothelial system organs (liver or spleen) retained these functionalized SWNTs and were rapidly eliminated from systemic blood circulation through the renal excretion route. In comparison, Cherukuri *et al* measured the blood elimination kinetics of water-soluble SWNTs in rabbits. In this assay the SWNTs were non-covalently coated with surfactant Pluronic F108 and the coating was found to be displaced by blood proteins within seconds. The SWNT concentration in the blood serum decreased exponentially with a half-life of $\sim$1 h and no adverse effects were discovered for low-level nanotube exposure from either behavior or pathological examination [76].

These current studies underscore the critical need for a comprehensive risk assessment of carbon nanomaterials for the healthy development of nanotechnology. This assessment, as pointed out by a recent commentary in Nature, entitled 'Safe handling of nanotechnology' [77]. This 'cradle to grave' approach that they suggest may require a decade to complete to thoroughly describe the synthesis, exposure, uptake, transport, and disposal of engineered

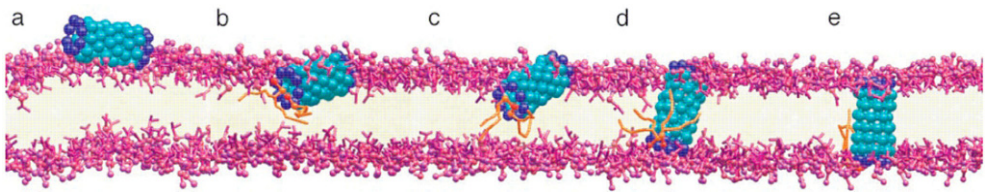

Figure 10. Sequence of the spontaneous insertion of nanotube with hydrophilic termini (NT*) into a model lipid bilayer. NT* molecule adsorbs onto the membrane (a). Partial immersion subsequently occurs and a few lipids form salt bridges with the hydrophilic termini of the tube (b). Next, thermal fluctuations drive one end of the NT* toward the membrane core (c). The flanking lipids and the hydrophilic terminus interact with the opposite side of the membrane (d). The escort lipids detach from the hydrophilic terminus, thereby allowing the formation of a transmembrane pore (e) [78] (© National Academy of Sciences).

nanomaterials. The impact of such assessment encompasses not only cell biology and nanomedicine but also healthcare and environment control. The following section details our MD simulations on fullerene translocation across a lipid bilayer and our experimental study on the biomodification of lipid-coated SWNTs by *Daphnia magna*, a model aquatic organism.

4.1. MD simulations on translocation of fullerene and its derivatives

The cell membrane is arguably the most important component of any living cell. It provides partition between inter-cellular and intra-cellular environment and selective transport mechanisms. Therefore, understanding the interaction between nanomaterials and cell membranes, and the translocation of nanomaterials through these membranes is a critical step towards a thorough and mechanistic understanding of the cytotoxicity of nanomaterials.

Interactions between carbon nanomaterials and cell membrane have been studied from different perspectives in recent years. Coarse-grained MD simulations have been used to study the spontaneous insertion of carbon nanotube into the cell membrane [78]. In these simulations, the carbon nanotube was functionalized by hydrophilic termini at both ends. Figure 10 shows the sequence of the nanotube insertion; a two-step insertion process is clearly evident. Specifically, during the insertion process, the nanotube first adsorbs onto the membrane plane, and then reorients to adopt a transmembrane configuration. During this process, it was found that the transport of the hydrophilic tube end across the membrane was facilitated by the chaperone lipids undergoing trans-bilayer flips. A more comprehensive study of the insertion of nanotube with different functionalization and the transport of water through nanotube was subsequently reported in [79]. Interestingly, it was also found that though a completely hydrophobic nanotube can enter the bilayer easily, the formation of transmembrane pores by the nanotube, as observed for nanotube with hydrophilic termini functionalization, was not observed during the simulation (see figure 11). Such a study highlights the importance of lipid–nanotube interaction in determining the translocation properties of nanotubes. The insertion of carbon nanotube into the membrane is expected to cause local structural changes. In particular, the length of the hydrophobic portion of a nanotube plays a critical role in determining the final conformation of the nanotube inside the membrane and the conformation of membrane bilayer near the adsorption site. Prior studies indicate that if there is such a mismatch between the hydrophobic portion of the insertion peptide and the lipid bilayer (termed 'hydrophobic mismatch'), a swelling/compression of bilayer and tilting of insertion peptide can be induced [80–83]. Such phenomena were explored thoroughly for nanotube insertion in [84],

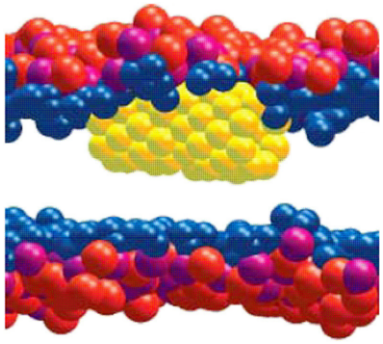

Figure 11. Adsorption of a completely hydrophobic nanotube into a model lipid bilayer [79] (© Biophysical Society).

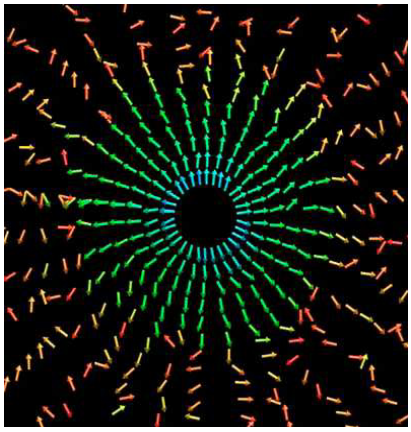

Figure 12. Lipid ordering around an eight-ring transmembrane nanotube. The field of lipid head-to-tail vectors is projected into the membrane plane around an eight-ring narrow nanotube. The intensity reduces from the center to the outer radius [84] (© Biophysical Society).

and similar behaviors caused by the peptide insertion were reported. Because of the rigidity of the nanotube, a layering of lipids around the insertion nanotube extending approximately 1.5 nm into the bulk lipids was detected. A strong ordering of the lipid tail-to-head vector in the membrane plane was also detected, most clearly seen in figure 12 for an eight-ring nanotube. Such an ordering is a result of formation of lipid meniscus around the tube and the tilting of these lipid molecules. The ordering was found to extend about 2.0 nm from the nanotube center in the membrane plane, and increased as the length of the tube decreased or as the radius of the tube increased.

Coarse-grained MD simulation is very effective in elucidating the overall picture of the nanotube–membrane interactions, and is especially useful for studying behavior of large tubes at long timescales. For smaller nanoparticles, however, it is advantageous to model the system with atomistic resolution. By complementing the atomistic simulation results with statistical analysis, it is possible to explore the nanoparticle–membrane interaction at long timescales. A full MD simulation of the interaction between a model membrane and combustion-generated carbon nanoparticles was reported in [85]. It was found that the shape and size of the nanoparticle plays a very important role in the membrane–particle interactions. Specifically,

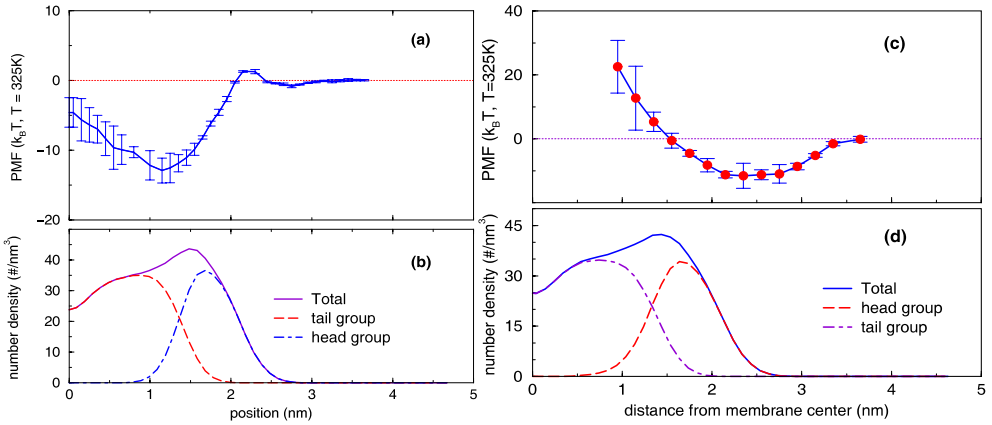

Figure 13. Panels (a) and (c): potential of mean force of pristine and functionalized buckyballs across a DPPC membrane bilayer. Panels (b) and (d): number density of lipid molecules in the transmembrane direction for membrane interacting with pristine and functionalized buckyball, respectively. Because of the symmetry, only data for the upper bilayer leaflet is shown [72] (© American Chemical Society).

the adsorption of carbon particle on the membrane enhances as the particle size increases, and elongated particles seem to enter the membrane much more easily, as compared to their round counterparts with the same molecular weight. Water molecules were also reported to be trapped into the membrane. Although it is not clear whether such trapping is caused by the pulling of the nanoparticle between sampling positions employed in their simulations,, this phenomenon seems to be supported by the experimental observation that membranes can become leaky upon contact with nanoparticles [71]. We recently reported the comparative study of the interaction and translocation behavior of pristine and functionalized buckyball (C_{60}) through a model cell membrane [72]. The study was motivated by the experiments in [71] where functionalization was found to significantly affect the cytotoxicity. The simulation results indicate that while a pristine C_{60} molecule can readily jump into the bilayer with a mean speed on the order of several meters per second, its functionalized counterpart $C_{60}(OH)_{20}$ tends to adsorb on the membrane surface. To explain the origin of the different interaction behaviors and to estimate the mean translocation time of the different C_{60} through the membrane, we computed the potential of mean force (PMF) of the buckyball across the membrane bilayer. Figure 13 compares the PMFs for the two different forms of buckyball. We observe that while PMF for the pristine buckyball has a slight barrier just outside the bilayer, it is approximately 12 k_BT lower than the bulk at position 1.1 nm from the bilayer center. Such a PMF profile significantly differs from that for a functionalized buckyball which shows a deep valley ($\sim$11 k_BT) near the membrane surface and increases dramatically as it approaches the bilayer center. The difference in the PMF is mainly due to the fact that the functionalization renders the buckyball hydrophilic. This leads to a stronger affinity between the buckyball and the head groups of the bilayer, while the pristine buckyball has a stronger affinity to the hydrophobic interior of the membrane bilayer. By computing the diffusion coefficient of the buckyballs inside the membrane bilayer, we estimated that the pristine buckyball can translocate the bilayer within a few milliseconds, while the mean translocation time for its functionalized counterpart is eight orders of magnitude longer. To study the impact of fullerene on the structure of the membrane bilayer, we tessellated the membrane bilayer and computed the average area per lipid head as a function of the lateral distance between the buckyball and lipid head. Figure 14(a) shows the

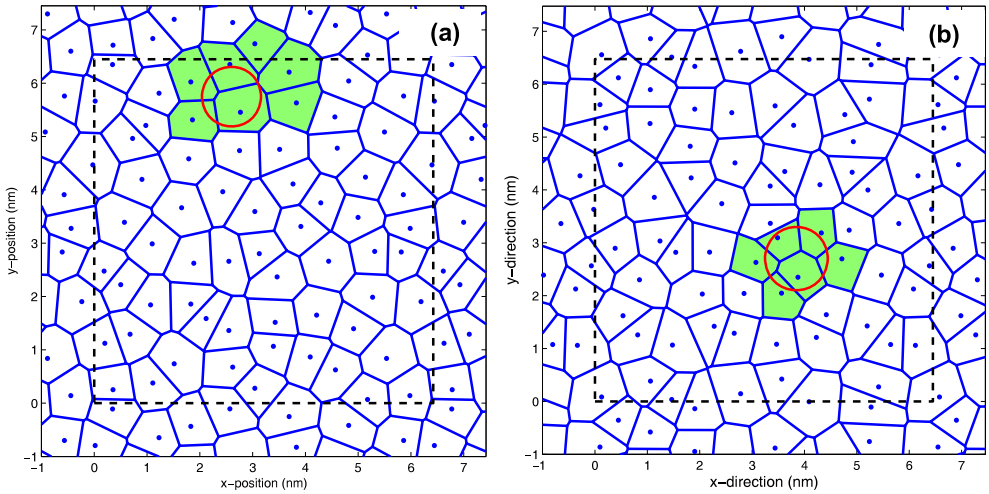

Figure 14. Representative Voronoi tessellation of membrane bilayers interacting with fullerene. (a) when a pristine buckyball is adsorbed at a relatively shallow position inside the bilayer (distance between buckyball center to the bilayer central plane is 1.2 nm) and (b) when a $C_{60}(OH)_{20}$ molecule is adsorbed on the membrane surface. The dots denote the center of mass of the DPPC head groups and the circle (diameter: 1.2 nm) denotes the projection of the $C_{60}(OH)_{20}$ molecule on the membrane plane. The shaded cells denote the lipid head groups that are adjacent to the $C_{60}(OH)_{20}$ molecule. The dashed line denotes the periodic boundary [72] (© American Chemical Society).

typical situation of the membrane when the pristine buckyball is adsorbed in a relatively shallow position inside the membrane and figure 14(b) shows the typical situation of the membrane when the functionalized buckyball is adsorbed on the membrane. We observed that the pristine buckyball adsorbed shallowly inside the bilayer tends to increase the area of the lipid head adjacent to it, and thus facilitates the formation of micropores. The functionalized buckyball, however, appears to 'pinch' the membrane, and thus prevents the formation of micropores on the membrane. Since the formation of micropores may enhance the mass transfer of large-sized penetrants and cause membrane leakage and cytotoxicity, the above results offer a physical mechanism for the reduced cytotoxicity of functionalized buckyball as reported in [71]. These findings highlight the effects of surface functionalization on the interactions between cell membranes and nanomaterials. The demonstrated physical interactions complement the chemical and biological mechanisms of membrane leakage (e.g. via oxidative damage of lipids). However, the relative importance of the physical mechanism as compared to the earlier reported mechanism remains to be elucidated.

4.2. Biomodification of lipid-coated SWNT by Daphnia

Among the many problems regarding the integration of nanomaterials with biological systems, the inherent insolubility of nanomaterials in aqueous solutions presents one of the greatest challenges. It is a major problem that must be resolved so that an accurate and systematic characterization of nanotoxicity can be done. Most of the current research in the nascent field of nanotoxicology overlooks this issue. Indeed, nanotoxicity is consistently confused with the toxicity caused by microparticles and macroparticles (e.g., catalyst particles such as nickel and iron, and amorphous carbons) in pristine nanomaterials. On the other hand, from the environmental viewpoint, water-soluble nanomaterials are of greater concern than their non-soluble counterparts due to increased mobility.

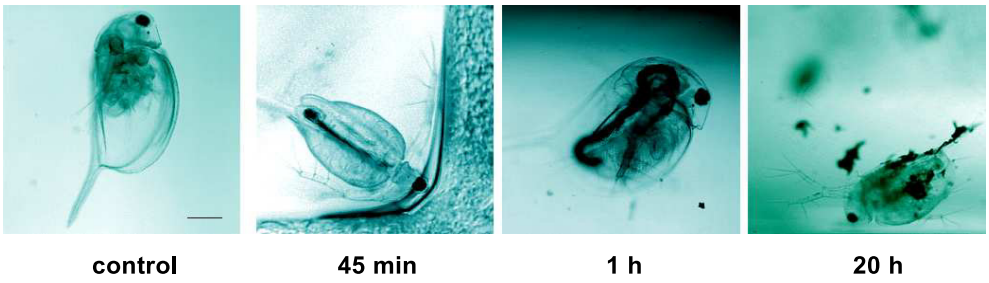

Figure 15. Time course of *Daphnia magna* exposed to SWNT–LPC (5 mg l^{-1} for SWNTs). The weight ratio of LPC:SWNT is 5:1. Note the large numbers of tubes filling the gut track at 45 min and 1 h. Also note the clumps of precipitated tubes around the daphnid after 20 h of exposure (scale bar: 200 μm) [39] (© American Chemical Society).

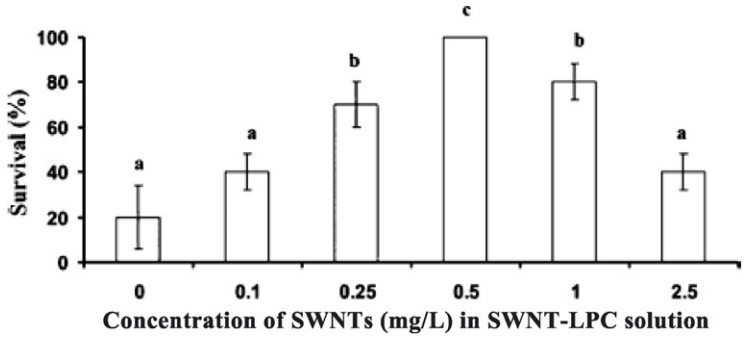

Figure 16. Mean per cent survival of *Daphnia magna* exposed to SWNT–LPC under starvation conditions (no algae–YTC food) for 96 h (letters denote statistical significance; $\alpha = 0.05$). Note the hormetic response at concentrations below 0.5 mg l^{-1} SWNT–LPC and manifested toxicity in concentrations above 0.5 mg l^{-1} SWNT–LPC. *X*-axis concentrations listed above refer to the concentration of SWNTs in solution (solutions contain a 5:1 LPC:SWNT mass ratio) [39] (© American Chemical Society).

We have examined the nanotoxicity of SWNT solubilized by lysophospholipids [39]. We measured the uptake and elimination of SWNT–LPC *in* water flea, *Daphnia magna*, an aquatic model organism. We found that *Daphnia magna* ingested nanotubes through normal feeding behavior and utilize the lysophophatidylcholine coating as a food source. We also noticed that *Daphnia magna* were able to modify the solubility of the nanotubes, likely through digestion of the lipid coating (figure 15, the panel for 20 h incubation). This modification significantly altered the physical properties of SWNTs in freshwater. Acute toxicity was observed only in the highest test concentrations of 0.5 mg l^{-1} under starvation conditions (figure 16) [39].

After the ingestion of lipid LPC, SWNTs were no longer water soluble and were observed to accumulate on the external surface of the daphnid (figure 15, right panel). In several bioassays, we observed that this accumulation prevented the organisms from moving through the water column and, in some cases, were enough to hold them to the bottom of the exposure chamber. Accumulation at such high levels would almost certainly result in a decreased ability to feed with the resultant chronic deleterious effects that could account for a biophysical mechanism of toxicity. It is likely that the extra mass adhered to the organism would have energetic effects in the long term, resulting in decreased growth and decreased or delayed reproduction [39]. Therefore, studies on these types of effects resulting from chronic exposure as well as studies investigating potential cellular toxicity from chronic exposure are needed.

5. Summary and outlook

Much new knowledge and even more excitement has been generated about nanomaterials over the past several years, and much more remains to be done to thoroughly understand their functions in biological systems. The great challenges presented by the interactions between nanomaterials and biological and environmental systems, willingly or unwillingly, have opened vast venues for fundamental and applied science and engineering, whose endpoints are focused at the nanoscale. In this review the authors attempt to illustrate both the rich physics in deciphering the complex roles of nanomaterials in biological systems, and to emphasize the inseparable relation between the solubility, bioavailability, and toxicity of nanomaterials. The justification for this emphasis is twofold. First, the literature indicates that the same nanomaterials can deliver different or even contrary effects to biological systems, possibly due to the physical and chemical modifications to the materials by biomolecules and biomolecular complexes. Second, there is an urgent need to advance our ability to mitigate nanotoxicity, which must be done for development of nanotechnologies to occur. Only a joint and multidisciplinary endeavor can ensure the continued scientific, environmental, and societal development of safe and dependable nanomaterials. We envision the major efforts of physics lie in the experimental detection and theoretical analysis of the thermal, electronic, and optical properties of nanomaterials, and in determining the conformational and energetic states of biological systems to infer their interaction. Such studies will facilitate the biochemical, biological, and toxicological studies on deciphering the biological responses to nanomaterials. New development in advanced microscopy and spectroscopy techniques as well as in atomistic and molecular statistics will find ample use for such applications.

Acknowledgments

Ke thanks his students Sijie Lin, Qi Lu, Jessica Moore, Marcus Allegood, and Donovan Jones and his co-workers Professors Apparao Rao, Stephen Klaine, Yonnie Wu, Aaron Roberts, Lyndon Larcom, and Andrew Mount for their invaluable contributions to the work highlighted in this article. Ke acknowledges an ACS PRF grant No. 45214-G7 and a research investment fund from Clemson University. Both Ke and Qiao acknowledge NSF-SGER grants Nos BES-0630823 and CBET-0736037, the results of which are also detailed in this paper. This article was proofread by Godfrey Kimball and Emma Neff.

References

[1] Chen R J, Bangsaruntip S, Drouvalakis K A, Kam N W S, Shim M, Li Y, Kim W, Utz P J and Dai H J 2003 *Proc. Natl Acad. Sci. USA* **100** 4984
[2] Wang J, Liu G, Jan M R and Zhu Q 2003 *Electrochem. Commun.* **5** 1000
[3] Mitchell D T, Lee S B, Trofin L, Li N, Nevanen T K, Söderlund H and Martin C R 2002 *J. Am. Chem. Soc.* **124** 11864
[4] Park K H, Chhowalla M, Iqbal Z and Sesti F 2003 *J. Biol. Chem.* **278** 50212
[5] Hu H, Ni Y, Montana V, Haddon R C and Parpura V 2004 *Nano Lett.* **4** 507
[6] Wang J, Liu G and Jan M R 2004 *J. Am. Chem. Soc.* **126** 3010
[7] Sitharaman B *et al* 2005 *Chem. Commun.* 3915
[8] Pantarotto D, Briand J, Prato M and Bianco A 2004 *Chem. Commun.* 16
[9] Pantarotto D, Singh R, McCarthy D, Erhardt M, Braind J-P, Prato M, Kostarelos K and Bianco A 2004 *Angew. Chem.* **43** 5242
[10] Kam N W S, Jessop T C, Wender P A and Dai H J 2004 *J. Am. Chem. Soc.* **126** 6850
[11] Liu Y, Wu D C, Zhang W D, Jiang X, He C B, Chung T S, Goh S H and Leong K W 2005 *Angew. Chem.* **44** 4782
[12] Lu Q, Moore J M, Huang G, Mount A S, Rao A M, Larcom L L and Ke P C 2004 *Nano Lett.* **4** 2473

[13] Bullard-Dillard R, Creek K E, Scrivens W A and Tour J M 1996 *Bioorg. Chem.* **24** 376
[14] Cagle D W, Kennel S J, Mirzadeh S, Alford J M and Wilson L J 1999 *Proc. Natl Acad. Sci. USA* **96** 5182
[15] Lacerda L, Bianco A, Prato M and Kostarelos K 2006 *Adv. Drug Delivery Rev.* **58** 1460
[16] Hwang K C and Mauzerall D 1993 *Nature* **361** 138
[17] Niu S and Mauzerall D 1996 *J. Am. Chem. Soc.* **118** 5791
[18] Dugan L L, Turetsky D M and Du C 1997 *Proc. Natl Acad. Sci. USA* **17** 9434
[19] Sijbesma R, Srdanov G, Wudl F, Castoro J A, Wilkins C, Friedman S H, DeCamp D L and Kenyon G L 1993 *J. Am. Chem. Soc.* **115** 6510
[20] Gharbi N, Pressac M, Hadchouel M, Szwarc H, Wilson S R and Moussa F 2005 *Nano Lett.* **5** 2578
[21] Wharton T and Wilson L J 2002 *Tetrahedron Lett.* **43** 561
[22] Ashcroft J M, Tsyboulaski D A, Hartman K B, Zakharian T Y, Marks J W, Weisman R B, Rosenblum M G and Wilson L J 2006 *Chem. Commun.* 3004
[23] Sano M, Kamino A, Okamura J and Shinkai S 2001 *Langmuir* **17** 5125
[24] Banerjee S and Wong S S 2002 *J. Am. Chem. Soc.* **124** 8940
[25] Pompeo F and Resasco D E 2002 *Nano Lett.* **2** 369
[26] Bahr J L, Mickelson E T, Bronikowski M J, Smalley R E and Tour J M 2001 *Chem. Commun.* **1** 193
[27] Sun Y, Wilson S R and Schuster D I 2001 *J. Am. Chem. Soc.* **123** 5348
[28] Pantarotto D, Partidos C D, Hoebeke J, Brown F, Kramer E, Briand J P, Muller S, Prato M and Bianco A 2003 *Chem. Biol.* **10** 961
[29] Shim M, Kam N W S, Chen R J and Dai H J 2002 *Nano Lett.* **2** 285
[30] Matarredona O, Rhoads H, Li Z R, Harwell J H, Balzano L and Resasco D E 2003 *J. Phys. Chem.* B **107** 13357
[31] Yurekli K, Mitchell C A and Krishnamoorti R 2004 *J. Am. Chem. Soc.* **126** 9902
[32] O'Connell M J *et al* 2002 *Science* **297** 593
[33] O'Connell M J, Boul P, Ericson L M, Huffman C, Wang Y, Haroz E, Kuper C, Tour J, Ausman K D and Smalley R E 2001 *Chem. Phys. Lett.* **342** 265
[34] Rao R, Lee J, Lu Q, Keskar G, Freedman K O, Floyd W C, Rao A M and Ke P C 2004 *Appl. Phys. Lett.* **85** 4228
[35] Strano M S, Zheng M, Jagota A, Onoa G B, Heller D A, Barone P W and Usrey M L 2004 *Nano Lett.* **4** 543
[36] Wang H, Zhou W, Ho D L, Winey K I, Fischer J E, Glinka C J and Hobbie E K 2004 *Nano Lett.* **4** 1789
[37] Zheng M, Jagota A, Semke E D, Diner B A, McLean R S, Lustig S R, Richardson R E and Tassi N G 2003 *Nat. Mater.* **2** 338
[38] Wu Y, Hudson J S, Lu Q, Moore J M, Mount A S, Rao A M, Alexov E and Ke P C 2006 *J. Phys. Chem.* B **110** 2475
[39] Roberts A P, Mount A S, Seda B, Qiao R, Lin S, Ke P C, Rao A M and Klaine S J 2007 *Environ. Sci. Technol.* **41** 3025 (ASAP)
[40] Didenko V V, Moore V C, Baskin D S and Smalley R E 2005 *Nano Lett.* **5** 1563
[41] Lu Q, Freedman K O, Rao R, Huang G, Lee J, Larcom L L, Rao A M and Ke P C 2004 *J. Appl. Phys.* **96** 6772
[42] Georgakilas V, Tagmatarchis N, Pantarotto D, Bianco A, Briand J P and Prato M 2002 *Chem. Commun.* 3050
[43] Huang W, Taylor S, Fu K, Lin Y, Zhang D, Hanks T W, Rao A M and Sun Y P 2002 *Nano Lett.* **2** 311
[44] Erlanger B F, Chen B X, Zhu M and Brus L 2001 *Nano Lett.* **1** 465
[45] Chen R J, Zhang Y, Wang D and Dai H J 2001 *J. Am. Chem. Soc.* **123** 3838
[46] Bachilo S M, Strano M S, Kittrell C, Hauge R H, Smalley R E and Weisman R B 2002 *Science* **298** 2361
[47] Richard C, Balavoine F, Schultz P, Ebbesen T W and Mioskowski C 2003 *Science* **300** 775
[48] Qiao R and Ke P C 2006 *J. Am. Chem. Soc.* **128** 13656
[49] Lindahl E, Hess B and van der Spoel D 2001 *J. Mol. Mod.* **7** 306
[50] Islam M F, Rojas E, Bergey D M, Johnson A T and Yodh A G 2003 *Nano Lett.* **3** 269
[51] Andrievsky G V, Klochkov V K, Bordyuh A and Dovbeshko G I 2002 *Chem. Phys. Lett.* **364** 8
[52] Arbogast J W and Foote C S 1991 *J. Am. Soc. Chem.* **113** 8886
[53] Ma B and Sun Y P 1996 *J. Chem. Soc., Perkin Trans.* **2** 2157
[54] Graja A and Farges J P 1998 *Adv. Mater. Opt. Electron.* **8** 215
[55] Harigaya K and Abe S 1994 *Phys. Rev.* B **49** 16746
[56] Harigaya K and Abe S 1996 *J. Phys.: Condens. Matter* **8** 8057
[57] Gandhi N M and Nair C K K 2005 *Mol. Cell. Biochem.* **278** 111
[58] Labieniec M and Gabryelak T 2006 *J. Photochem. Photobiol.* B **82** 72
[59] Aissaoui A *et al* 2002 *Curr. Drug Targets* **3** 1
[60] Dubruel P, Christiaens B, Rosseneu M, Vandekerckhove J, Grooten J, Goossens V and Schacht E 2004 *Biomacromolecules* **5** 379
[61] Allen T M and Cullis P R 2004 *Science* **303** 1818
[62] Verma I and Somia N 1997 *Nature* **389** 239

[63] Kam N W S, Liu Z and Dai H J 2005 *J. Am. Chem. Soc.* **127** 12492
[64] Kam N W S and Dai H J 2005 *J. Am. Chem. Soc.* **127** 6021
[65] Kam N W S, O'Connell M, Wisdom J A and Dai H J 2005 *Proc. Natl Acad. Sci. USA* **102** 11600
[66] Heller D A, Jeng E S, Yeung T K, Martinez B M, Moll A E, Gastala J B and Strano M S 2006 *Science* **311** 508
[67] Lin S, Keskar G, Wu Y, Wang X, Mount A S, Klaine S J, Moore J M, Rao A M and Ke P C 2006 *Appl. Phys. Lett.* **89** 143118-1
[68] Shvedova A A, Castranova V, Kisin E R, Schwegler-Berry D, Murray A R, Gandelsman V Z, Maynard A and Baron P 2003 *J. Toxicol. Environ. Health* A **66** 1909
[69] Warheit D B, Laurence B R, Reed K L, Roach D H, Reynolds G A M and Webb T R 2004 *Toxicity Sci.* **77** 117
[70] Lam C W, James J T, McCluskey R and Hunter R L 2004 *Toxicity Sci.* **77** 126
[71] Sayes C M *et al* 2004 *Nano Lett.* **4** 1881
[72] Qiao R, Roberts A P, Mount A S, Klaine S J and Ke P C 2007 *Nano Lett.* **7** 614 (ASAP)
[73] http://nanotechweb.org/articles/news/4/11/3/1
[74] Manna S K, Sarkar S, Barr J, Wise K, Barrera E V, Jejelowo O, Rice-Ficht A C and Ramesh G T 2005 *Nano Lett.* **5** 1676
[75] Singh R, Pantarotto D, Lacerda L, Pastorin G, Klumpp C, Prato M, Bianco A and Kostarelos K 2006 *Proc. Natl Acad. Sci. USA* **103** 3357
[76] Cherukuri P, Gannon C J, Leeuw T K, Schmidt H K, Smalley R E, Curley S A and Weisman R B 2006 *Proc. Natl Acad. Sci. USA* **103** 18882
[77] Maynard A D 2006 *Nature* **444** 267
[78] Lopez C F, Nielsen S O, Moore P B and Klein M L 2004 *Proc. Natl Acad. Sci. USA* **101** 4431
[79] Lopez C F, Nielsen S O, Ensing B, Moore P B and Klein M L 2005 *Biophys. J.* **88** 3083
[80] de Planque M R R and Killian J A 2003 *Mol. Membr. Biol.* **20** 271
[81] Killian J A 1998 *Biochim. Biophys. Acta* **1376** 401
[82] Nielsen S O, Lopez C F, Ivanov I, Moore P B, Shelley J C and Klein M L 2004 *Biophys. J.* **87** 2107
[83] Kandasamy S K and Larson R G 2006 *Biophys. J.* **90** 2326
[84] Nielsen S O, Ensing B, Oritz V, Moore P B and Klein M L 2005 *Biophys. J.* **88** 3822
[85] Chang R and Violi A 2006 *J. Phys. Chem.* B **110** 5073